Abcb10 Role in Heme Biosynthesis *In Vivo*: Abcb10 Knockout in Mice Causes Anemia with Protoporphyrin IX and Iron Accumulation

Masatatsu Yamamoto,[a] Hiroshi Arimura,[b] Tomoko Fukushige,[c] Kentarou Minami,[d] Yukihiko Nishizawa,[d] Akihide Tanimoto,[e] Takuro Kanekura,[c] Masayuki Nakagawa,[b] Shin-ichi Akiyama,[a] Tatsuhiko Furukawa[a]

Department of Molecular Oncology,[a] Department of Urology,[b] Department of Dermatology,[c] Department of Clinical Pharmacy and Pharmacology,[d] and Department of Molecular and Cellular Pathology,[e] Graduate School Medical and Dental Sciences, Kagoshima University, Kagoshima, Japan

Abcb10, member 10 of the ABC transporter family, is reportedly a part of a complex in the mitochondrial inner membrane with mito-ferrin-1 (Slc25a37) and ferrochelatase (Fech) and is responsible for heme biosynthesis *in utero*. However, it is unclear whether loss of Abcb10 causes pathological changes in adult mice. Here, we show that $Abcb10^{-/-}$ mice lack heme biosynthesis and erythropoiesis abilities and die in midgestation. Moreover, we generated $Abcb10^{F/-}$; *Mx1-Cre* mice, with $Abcb10$ in hematopoietic cells deleted, which showed accumulation of protoporphyrin IX and maturation arrest in reticulocytes. Electron microscopy images of $Abcb10^{-/-}$ hemato-poietic cells showed a marked increase of iron deposits at the mitochondria. These results suggest a critical role for Abcb10 in heme biosynthesis and provide new insights into the pathogenesis of erythropoietic protoporphyria and sideroblastic anemia.

Heme plays a critical role in various biological processes. Thus, failure of heme biosynthesis causes severe inherited or ac-quired disorders in humans (1). Biosynthesis of heme consists of the eight-step reaction pathway involving both the mitochondria and the cytoplasm. The delta-aminolevulinate synthase gene (*ALAS*), which codes for the first enzyme in the heme biosynthetic pathway, was identified as being responsible for X-linked sidero-blastic anemia (XLSA) (2, 3). Additionally, the final step of the heme biosynthetic pathway, the insertion of iron into protopor-phyrin IX (PPIX) to produce heme, is catalyzed by ferrochelatase (FECH), which is localized in the mitochondrial inner membrane (4, 5). Erythropoietic protoporphyria (EPP) is an inherited disor-der caused by partial FECH deficiency (6). Iron, the prosthetic atom of the heme group, is imported into the mitochondrial matrix by mitoferrin (Slc25a37) and is required for embryonic hematopoiesis (7, 8). Both Fech and Slc25a37 have been shown to interact with Abcb10, which functions to stabilize an oligomeric complex (5, 9). Abcb10, a mitochondrial inner membrane ATP-binding cassette transporter, was found to be a key protein that is highly induced by GATA1 and is involved in heme production during mouse erythroleukemia cell differentiation (10–12).

Recently, studies of *Abcb10* knockout (KO) mice have been reported. Since the loss of 1 allele of *Abcb10* led to an increase in damage to mitochondria and sarcoplasmic reticulum calcium ATPase, *Abcb10* heterozygous (+/−) mice showed an increased susceptibility to oxidative stress induced by ischemia and reperfu-sion. Therefore, Abcb10 was shown to determine the ability to tolerate cardiac ischemia/reperfusion (13). Further, *Abcb10* ho-mozygous (−/−) mice died during the embryonic stage because of increased apoptosis in $Abcb10^{-/-}$ erythroid precursor cells (14). Previous reports have also shown that *Abcb10* deletion re-sults in oxidative stress, leading to mitochondrial dysfunction; however, little is known regarding whether Abcb10 is associated with heme biosynthesis.

In this study, we inactivated the *Abcb10* gene in germ line and in adult hematopoietic cells in conditional *Abcb10* KO and 2 Cre transgenic mouse lines. The cytomegalovirus (CMV) enhancer containing a chicken beta-actin transcription start site and a rab-bit beta-globin intron fused with Cre (CAG-Cre) showed ubiqui-tous KO of *Abcb10* in all mouse tissue. In contrast, interferon-induced Cre (Mx1-Cre) showed KO of *Abcb10* in the liver, spleen, and bone marrow (BM). Here, we show that Abcb10 is essential for hematopoietic differentiation in both embryos and adults. Particularly, hematopoietic tissue-specific *Abcb10* KO mice showed high levels of PPIX accumulation in the erythrocytes and iron deposits in the mitochondria of BM cells (BMCs) as well as arrest of erythropoiesis at reticulocytes. These results indicate that Abcb10 plays a critical role in heme biosynthesis during insertion of iron into PPIX.

MATERIALS AND METHODS

Generation of mice carrying a conditional *Abcb10* allele ($Abcb10^{F/+}$) and hematopoietic tissue-specific inducible deletion of *Abcb10*. The murine *Abcb10* gene consists of 13 exons spread over more than 30 kb of mouse chromosome 8 on the reverse strand. We first planned to disrupt *Abcb10* mRNA through removal of exon 3.

The EagI fragment (11 kb) for the 5′ long arm and the EcoRI fragment (9.5 kb) for the 3′ short arm, each of which includes exons 2 to 5, were obtained from a bacterial artificial chromosome (BAC) clone library (Ad-vanced Geno Techs Co.). The targeting vector was constructed by inserting a *loxP-FRT* fragment and a *loxP*-pMC1 *neo-FRT-loxP* fragment upstream and downstream of exon 3 for Cre- or FLP-mediated recombination and positive selection, respectively. The diphtheria toxin A chain gene was inserted into the genomic fragment for negative selection (Fig. 1A).

After the targeting vector was transfected into TT2 embryonic stem (ES) cells, G418-resistant colonies were selected. Homologous recombi-nant clones were then serially assessed by using Southern blot analysis with a 3′ outside probe as previously described (15).

Two homologous recombinant cells were injected into C57BL/6 blas-
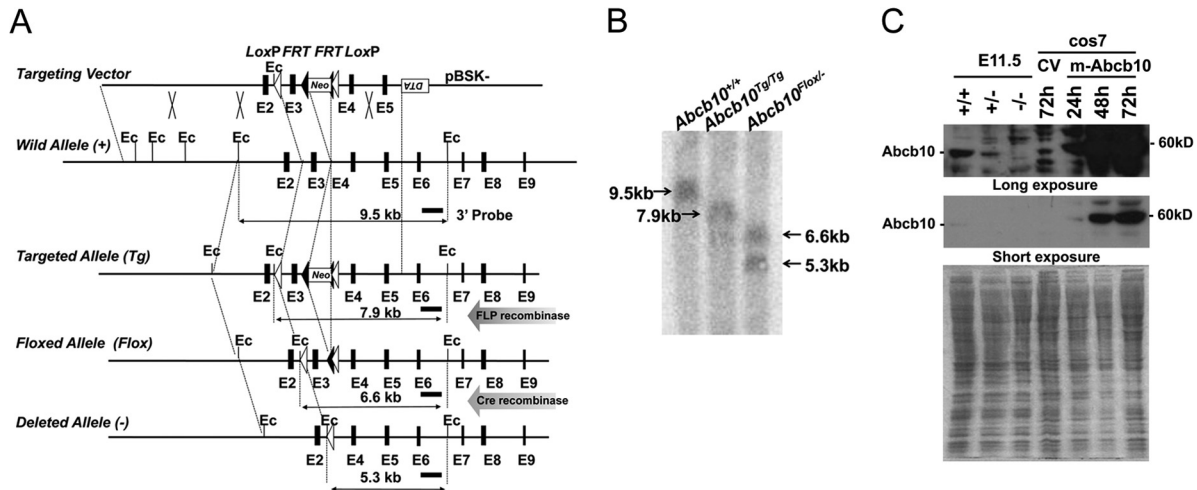
FIG 1 Generation of conditional *Abcb10* knockout mice and assessment of Cre- and FLP-mediated deletion. (A) Schematic representation of the targeting strategy. The figure shows the structure of the mouse *Abcb10* gene before and after its recombination with the targeting vector, after deletion of the *FRT-neo-FRT* cassette, and after further deletion of its floxed region. Positions of the *loxP* and *FRT* sites are designated by white and black triangles, respectively. The exons, deduced by comparison with the cDNA sequence, are denoted by black boxes (E2 to E9). The position of the 3′ external genomic DNA probe used for Southern blot analysis is bold and underlined (3′ Probe). EcoRI sites (Ec) are marked by vertical lines. The sizes and positions of the EcoRI fragments of each genome as detected by Southern blotting using the 3′ probe are indicated with bidirectional lines and numbers. (B) Cre-*loxP* and FLP-FRT-mediated deletion of the flanked *Abcb10* gene. Southern blot analysis (by using the 3′ probe shown in panel A) of DNA from *Abcb10*^{+/+}, *Abcb10*[Tg/Tg], and *Abcb10*[F/−] mice. The 5.3-kb fragment corresponding to the deleted allele (−) was observed only in *Abcb10*[Flox/−] mice. (C) Western blotting with anti-Abcb10 antibody of the whole embryo extract (E11.5) and mouse Abcb10-transfected Cos7 cells (upper, long exposure; middle, short exposure). The numbers under "CV" and "m-Abcb10" indicate numbers of hours after transfection. A sodium dodecyl sulfate (SDS) gel stained with Coomassie brilliant blue (CBB) shows that the same amount of protein (40 μg) was loaded in each lane (lower panel).

tocysts, resulting in male chimeric mice (F0). Next, the F0 generation was intercrossed to generate the targeted homozygous allele (*Abcb10*[Tg/Tg]).

To exclude the possibility that expression of *neo*[r] resulted in production of a particular phenotype, we crossed *Abcb10*[Tg/Tg] mice with CAG-FLP mice expressing FLP recombinase to generate a *neo*[−]-targeted allele (*Abcb10*[F/+]). The floxed allele homozygous mice (*Abcb10*[F/F]) were generated by intercrossing *Abcb10*[F/+] mice.

Mice with one of the *Abcb10* alleles knocked out (*Abcb10*^{+/−}) were obtained by mating F0 mice with the ubiquitous Cre-expressing strain of mice (*CAG-Cre*). *Abcb10*^{+/−} mice carrying an inducible *Cre* gene (*Abcb10*^{+/−}; *Mx1-Cre*) were obtained by mating *Mx1-Cre* mice with *Abcb10*^{+/−} mice.

Offspring in which the *Abcb10* allele had been deleted by inducible Cre expression in a hematopoietic tissue-specific manner (*Abcb10*[F/−]; *Mx1-Cre*) were bred by mating *Abcb10*^{+/−}; *Mx1-Cre* mice with *Abcb10*[F/F] mice. To induce deletion of the floxed *Abcb10* allele in *Abcb10*[F/−]; *Mx1-Cre* mice, Cre was induced under the control of the myxovirus resistance 1 (Mx1) promoter by use of intraperitoneal injections of poly(I·C) (pI-pC) double-stranded RNA (dsRNA) (250 μg/mouse; Sigma-Aldrich) 3 times at intervals of 2 days, unless otherwise indicated. Peripheral blood cells or BM cells were analyzed 2 days after the last pI-pC injection. For all parameters evaluated in this study, the phenotypes of *Abcb10*[F/+]; *Mx1-Cre*, *Abcb10*[F/−], and *Abcb10*[F/+] mice were indistinguishable from those of wild-type mice, regardless of the Cre strain used. *CAG-FLP*, *CAG-Cre*, and *Mx1-Cre* mice were obtained from the Center for Animal Resources and Development (CARD), Kumamoto University. All procedures involving animals were approved by the Animal Care Committee of Kagoshima University.

Mouse genotyping. Genotyping of the *Abcb10* alleles was performed by using Southern blot analysis and PCR. EcoRI-digested DNAs were used for Southern blotting, using genomic DNA probes from the region downstream of the 3′ arm (between exons 6 and 7) outside the targeting construct (Fig. 1A). For PCR, we used the oligonucleotide primers abcb10 7F (5′-CATGTACAGATTAATGCTCCAGGTC-3′) (sense) and abcb10 8R (5′-CAGTGCATTGAGGAATCACTAGGAAC-3′) (antisense) for the de-

leted allele, abcb10 8F (5′-AAGGTCATTCTTGGCTGCACAATCC-3′) (sense) and abcb10 8R for the floxed allele, and Cre1 (5′-ACATGTTCAG GGATCGCCAGG-3′) (sense) and Cre2 (5′-TAACCAGTGAAACAGCA TTGC-3′) (antisense) for the *Cre* transgenes.

Histology. Embryos or the tissues of adult mice were fixed in 10% phosphate-buffered formalin (pH 7.4), embedded in paraffin, cut into 8-μm sections, deparaffinized, and stained with standard hematoxylin and eosin (H&E; Muto Pure Chemicals) or Berlin blue (Wako Pure Chemicals) and nuclear fast red (Muto Pure Chemicals).

Immunostaining. After boiling for 20 min in 10 mM citric acid to activate the antigen and blocking for 30 min with 0.05% Tween 20 and 10% horse serum–phosphate-buffered saline (PBS) (working buffer) at room temperature, tissue slides were incubated with primary antibodies in working buffer overnight on 4°C, followed by incubation with secondary antibodies in working buffer for 1 h at room temperature. A polyclonal anti-cleaved caspase 3 antibody (Cell Signaling Technology) at 1:100 and a monoclonal antibromodeoxyuridine (anti-BrdU) antibody (BD Biosciences) at 1:200 were used as primary antibodies. Goat anti-rabbit or rabbit anti-mouse antibody (ABC Elite kit) was used as the secondary antibody according to the manufacturer's protocol (Vector Laboratories).

Construction and transfection of mouse *Abcb10* expression plasmid. The entire open reading frame of mouse *Abcb10* (accession no. BC054793.1) was inserted into the p3XFLAG-CMV-14 vector (Sigma-Aldrich) between the HindIII and SmaI sites. This expression vector was referred to as m-Abcb10. Transfection of m-Abcb10 or p3XFLAG-CMV-14 as a control vector (referred to as CV) into a Cos7 cell was conducted using 12 μg of DNA per plate and Lipofectamine (Life Technologies Corporation) according to the manufacturer's protocol.

Western blot analysis. Subcellular fractionation of mouse embryos and Cos7 cells transfected with m-Abcb10 or CV was conducted as described previously (16). Briefly, the samples were homogenized in 220 mM mannitol, 70 mM sucrose, and 5 mM potassium HEPES buffer, pH 7.5 (MSH). The homogenate was centrifuged at 600 × *g* for 10 min to precipitate the nuclei and cell debris, and the resulting supernatant fraction was centrifuged at 5,500 × *g* for 10 min to precipitate the mitochon-

drial fraction. The resulting supernatant fraction was composed of cytosol. Protein oxidation analysis was performed using the OxyBlot protein oxidation detection kit (Millipore). Carbonylated proteins were derivatized with 2,4-dinitrophenylhydladine (DNPH) according to the manufacturer's protocol. These samples were subjected to sodium dodecyl sulfate-polyacrylamide gel electrophoresis (SDS-PAGE) and electroblotted on polyvinylidene fluoride (PVDF) membranes. Western blot analysis was performed using anti-Abcb10 antibody (1:100) derived from the sera of a rabbit immunized with the mouse Abcb10 peptide (CRQPRLPFNEG MVLDEK), anti-heat shock protein 60 (anti-HSP60) (1:2,000; Cell Signaling), and anti-glyceraldehyde 3-phosphate dehydrogenase (anti-GAPDH) (1:10,000; Cell Signaling) as the primary antibody and a horseradish peroxidase (HRP)-conjugated goat anti-rabbit antibody (1:2,000; GE Healthcare) as the secondary antibody. Anti-Fech antibody (1:200; Santa Cruz Biotechnology) was used as a primary antibody, and an HRP-conjugated rabbit anti-goat antibody (1:2,000; GE Healthcare) was used as the secondary antibody.

OxyBlot analysis was performed using rabbit anti-2,4-dinitrophenyl (anti-DNP) antibody (1:150; Millipore) as a primary antibody.

Measurements of heme and PPIX. Heme level was measured using a heme assay kit (BioChain Institute, Inc.). To extract porphyrins, peripheral blood (0.5 ml) was mixed with 5 ml of ether-acetic acid (4:1, vol/vol), followed by centrifugation to remove the precipitate. The supernatant was then vortexed with 3 ml of 2.7 M HCl. The PPIX concentration in the lower aqueous acid layer was determined using high-performance liquid chromatography (HPLC) as described previously (17). Zn-PPIX and PPIX (Frontier Scientific) were used as the internal standard substance and the calibrator, respectively.

Electron microscopy. For ultrastructural analysis, specimens were fixed in 2.5% glutaraldehyde in phosphate-buffered saline and postfixed for 1 h in 2% buffered osmic acid solution. After dehydration with ethanol, tissues were embedded in epoxy resin (Epon 812; Taab Laboratories Equipment, Ltd.). Semithin sections were stained with toluidine blue, and ultrathin sections were contrasted with uranyl acetate and lead citrate. Stained sections were examined using an electron microscope (H-7650; Hitachi). For analytical electron microscopy, unstained ultrathin sections were inspected using a JEM-2500SE microscope (Jeol, Ltd.) to observe the sample surface architecture and inner structure as well as to contrast the image to reflect composition (i.e., scanning secondary electron image [SEI], light field scanning transmitted image [STEM-BF], and dark field scanning transmitted image [STEM-DF], respectively).

Peripheral blood count. $Abcb10^{F/-}$; $Mx1$-Cre mice and control mice were anesthetized with isoflurane. Blood was withdrawn from the heart using a 22-gauge needle. The syringes were coated with 0.5 M EDTA to prevent coagulation. The blood was immediately placed into EDTA-coated tubes and mixed thoroughly. Peripheral blood analysis was performed by the clinical pathology laboratory.

RESULTS

Targeted disruption of $Abcb10$. We generated mice with a conditional $Abcb10$ allele by use of a targeting construct designed to excise exon 3, which causes a frameshift mutation at the splice junction site across exons 2 and 4. This results in disruption of 3 transmembrane motifs and an ATP-binding domain that is encoded by the downstream region of exon 3 (Fig. 1A). The targeted and disrupted allele of the $Abcb10$ gene in mice was confirmed by using Southern blot analysis (Fig. 1B). Inactivation of Abcb10 in embryos was confirmed by using Western blot analysis, which showed that Abcb10 protein expression was dependent on the gene dosage in the embryonic genotype and was not detectable in $Abcb10^{-/-}$ mice (Fig. 1C).

Embryonic lethality of $Abcb10^{-/-}$ mice. Interbred $Abcb10^{+/-}$ mice yielded no null offspring among newborn mice. A reduction of $Abcb10^{-/-}$ genotype embryos to less-than-Mendelian ratios

TABLE 1 Embryonic lethality due to $Abcb10$ deletion[a]

Embryonic day	No. of mice with embryos of indicated genotype			No. of mice with resorption embryos
	+/+	+/−	−/−	
E9.5	7	16	6	0
E10.5	5	18	6	3
E11.5	6	8	3	3
Total	18	40	15	6

[a] The genotypes of $Abcb10$ embryos were derived from intercrossing $Abcb10^{+/-}$ mice. The numbers of mice with embryos of each genotype or with resorption embryos on the indicated embryonic days (E9.5 to E11.5) are shown. Genotype information for resorption embryos was not available.

and an increase in embryo resorption indicated that embryonic lethality in $Abcb10^{-/-}$ mice occurred between embryonic day 10.5 (E10.5) and E11.5 (Table 1.).

Compared with $Abcb10^{+/+}$ embryos at E11.5, $Abcb10^{-/-}$ embryos were noticeably paler due to the absence of hemoglobinized cells in the heart and fetal liver (Fig. 2A).

We examined the presence of hemoglobin and heme in these embryos by using benzidine staining and heme quantitative analyses. Benzidine-positive cells were present in abundance in the lumen of the heart and liver in $Abcb10^{+/+}$ embryos (Fig. 2B) but not in $Abcb10^{-/-}$ embryos. Additionally, a striking decrease in heme level was observed in the $Abcb10^{-/-}$ embryos compared with the level in $Abcb10^{+/+}$ embryos (Fig. 2C). These data suggest that $Abcb10^{-/-}$ embryos exhibit severely impaired heme biosynthesis followed by hemoglobin defects.

Abcb10 may play a role in heme biosynthesis by interacting with and stabilizing Fech, which is essential for inserting iron into the heme precursor (9). Thus, we assessed the status of Fech in $Abcb10^{-/-}$ embryos by using Western blot analysis. In the mitochondrial fraction, Fech protein expression in $Abcb10^{-/-}$ embryos was comparable to that in $Abcb10^{+/+}$ embryos. However, in the supernatant fraction, the Fech protein expression level in $Abcb10^{-/-}$ embryos was lower than that in $Abcb10^{+/+}$ embryos (Fig. 2D). Therefore, it appears that Abcb10 contributes to the stability of Fech prior to translocation into the mitochondria but does not affect the amount of Fech in mitochondria.

To evaluate embryonic cells, we investigated the proliferation and apoptosis of constituent cells in embryonic bodies (E11.5 embryos) by use of immunohistochemical analyses with the anti-BrdU antibody and anti-cleaved caspase 3 antibody. As shown Fig. 2E, $Abcb10^{+/+}$ embryos exhibited BrdU-positive cells, which were not observed in $Abcb10^{-/-}$ embryos. In contrast, a number of cells positive for cleaved caspase 3 were observed in the fetal livers of $Abcb10^{-/-}$ embryos, but no cleaved caspase 3-positive cells were present in $Abcb10^{+/+}$ embryos. These observations and the loss of hemoglobinized cells support the suggestion that $Abcb10^{-/-}$ embryos died because of embryonic hematopoietic failure.

$Abcb10^{-/-}$ hemocytes do not contain heme and contain free iron in the mitochondria. Next, we used Berlin blue staining to examine whether iron metabolism and trafficking properties differed depending on the $Abcb10$ genotype since iron is an essential ion of heme. $Abcb10^{-/-}$ embryos displayed significant iron accumulation in circulating cells (Fig. 2B).

To examine the appearance and localization of these iron deposits, we acquired transmission electron micrographs of
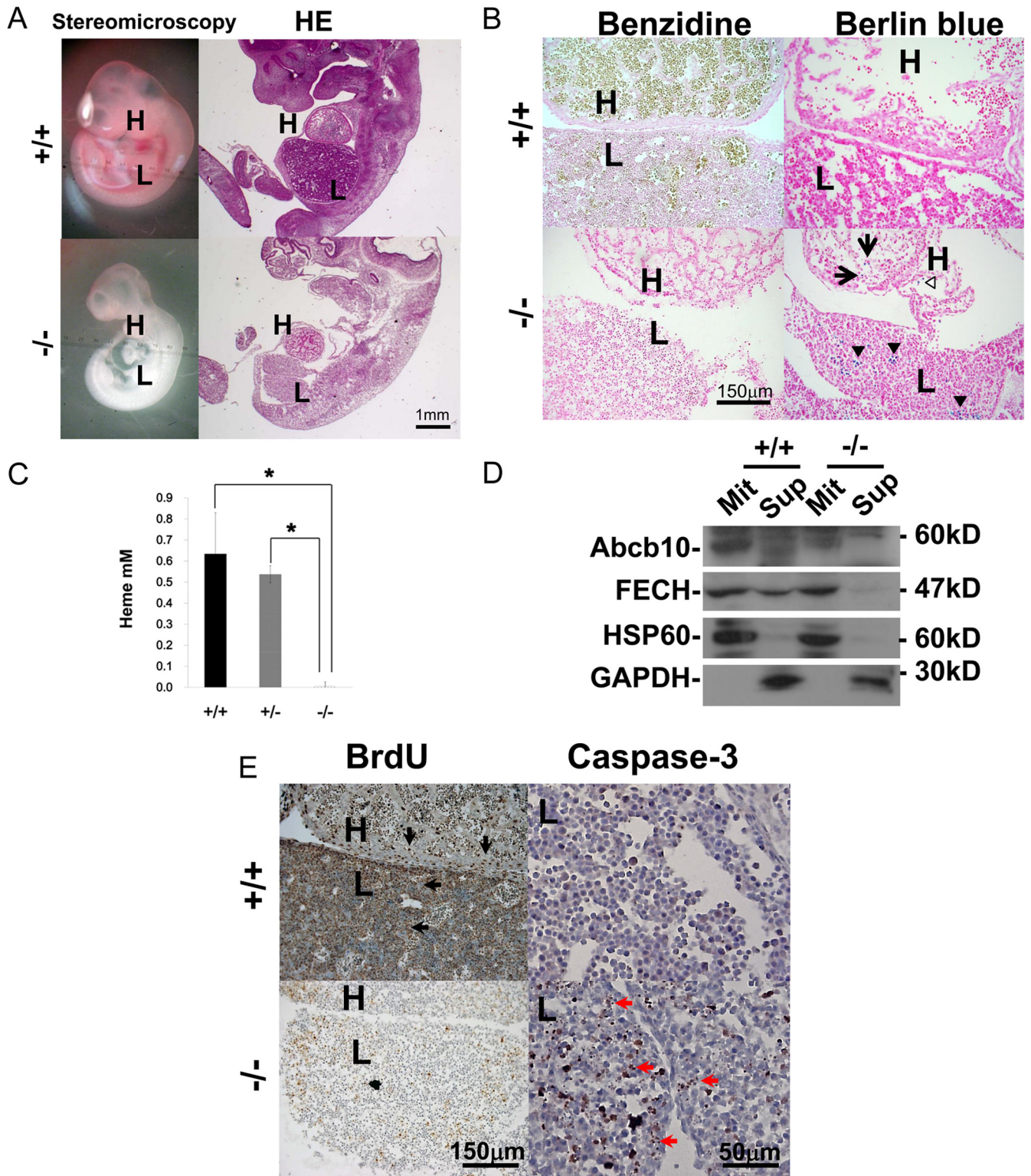
FIG 2 Comparative analysis of the morphology, hemoglobin, iron, and cell death in $Abcb10^{+/+}$ and $Abcb10^{-/-}$ mice. (A) Comparative morphological studies of $Abcb10^{+/+}$ (+/+) and $Abcb10^{-/-}$ (−/−) embryos. The left panels (+/+ and −/−) show stereomicroscopic images of E11.5 embryos. The −/− embryo is much paler than the +/+ embryo, including the heart (H) and liver (L). The right panels (+/+ and −/−) show hematoxylin-eosin (HE)-stained embryos. The −/− embryo shows faint eosin staining due to the sparseness of the cytosolic component followed by apoptosis in most of these cells (as shown in panel E). (B) Benzidine and Berlin blue-stained section of heart and liver from +/+ and −/− embryos. The benzidine stain showed hemoglobinized cells in +/+ but not in −/− embryos. In the Berlin blue stain, Fe-accumulating cells in the heart (arrows), vessels (open arrowhead), and liver (filled arrowheads) of only −/− embryos were stained in blue. (C) Total heme level of embryos. Data are expressed as the means ± standard deviations (SDs) of results from 3 embryos per genotype. +/−, $Abcb10$ heterozygous embryos; ∗, P values of <0.001. (D) Analyses for Fech and Abcb10 expressions in +/+ and −/− embryos. Western blot analyses of whole embryos were performed with antibodies against Abcb10, Fech, HSP60, and GAPDH. HSP60 and GAPDH were used as mitochondrial and supernatant fraction loading controls, respectively. Two hundred micrograms of protein for the mitochondrial fraction (Mit) and 70 μg protein for the supernatant fraction (Sup) were applied to the each lane. (E) Identification of growing and apoptotic cells by staining for BrdU in the heart (H) and the liver (L) or cleaved caspase 3 in the liver (L) from +/+ and −/− embryos.
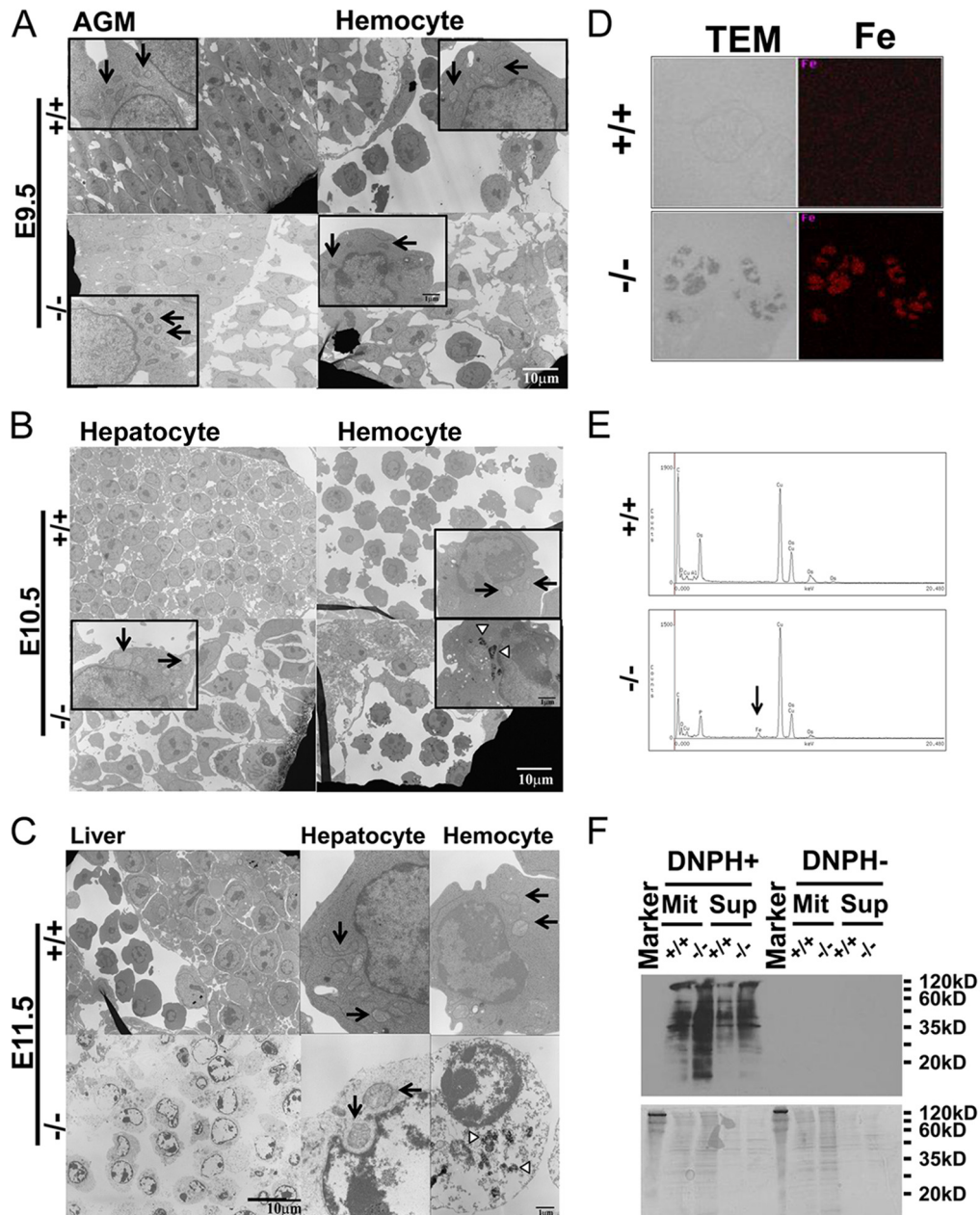
FIG 3 Analytical electron microscopy and ROS accumulation of $Abcb10^{-/-}$ embryos. (A to C) Electron micrographs of $+/+$ and $-/-$ embryonic hepatocytes (or the AGM region) and hemocyte at embryonic days 9.5, 10.5, and 11.5, respectively. Arrows show mitochondria, and arrowheads show strong electron-dense deposits in the mitochondrial matrix. All the subsets are higher magnificent images. (D and E) Data from analytical electron microscopy of $+/+$ and $-/-$ embryonic hemocytes at E10.5. (D) The transmission electron micrograph (TEM) (left) and the density of Fe (right) of the mitochondria of $+/+$ and $-/-$ embryonic hemocytes is shown. (E) Charts of elemental analysis from the field represented in panel D. The x axis indicates energy (keV), and the y axis indicates X-ray generation (count). The elements recognized by the analyzer are indicated at each peak. The arrow indicates the specific signal of Fe in $-/-$ embryonic hemocytes. (F) Comparison of protein oxidation in $+/+$ and $-/-$ embryos. The carbonylated proteins with oxidization stress were derived with DNPH and detected with anti-DNP antibody by use of the OxyBlot protein oxidation detection kit. Mit, 20 μg mitochondrial protein; Sup, 10 μg supernatant protein. The $+/+$ and $-/-$ embryos shown in panels A to F were obtained by breeding $Abcb10^{+/-}$ and $Abcb10^{+/-}$ mice. CBB-stained SDS-PAGE gel is shown at the bottom.

$Abcb10^{-/-}$ and $Abcb10^{+/+}$ embryos. In mice, hematopoiesis is autonomously initiated by the aorta-gonad-mesonephros (AGM) region at E9.5 (18). On this day, morphological differences in AGM region and circulating blood cells were not observed between $Abcb10^{-/-}$ and $Abcb10^{+/+}$ embryos (Fig. 3A). At E10.5 and E11.5, the $Abcb10^{+/+}$ embryo liver was composed of definite hematogenous tissues, but the $Abcb10^{-/-}$ embryonic liver showed

wide spaces between cells, indicating reduced cell-cell interactions (Fig. 3B and C). As shown in Fig. 3C, on E11.5, even in $Abcb10^{+/+}$ embryos, hematopoietic cells in the vessel remained immature since they preserved organelles (nuclei and mitochondria). However, strikingly, in $Abcb10^{-/-}$ embryos at E10.5 and E11.5, marked electron-dense materials, which localized to the mitochondria of hemocytes but not to hepatocytes, were observed (Fig. 3B and C).
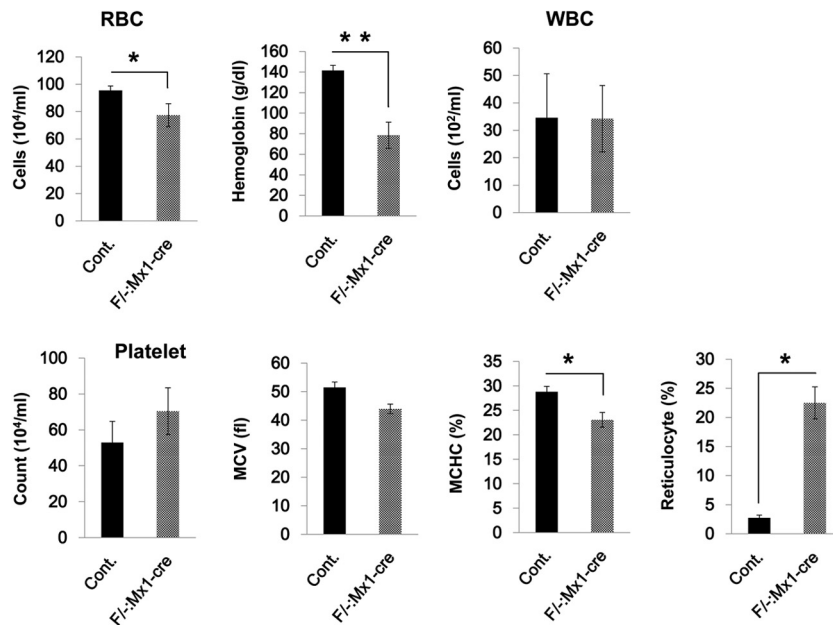
FIG 4 Mx1-Cre-mediated *Abcb10* deletion leads to anemia and impaired erythroid cell maturation in adult mice. Control (Cont.) ($n = 3$) and *Abcb10*$^{F/-}$; *Mx1-Cre* ($n = 9$) mice were subjected to peripheral blood counts. Results are shown as means ± SDs (error bars). RBC, red blood cell count; WBC, white blood cell count; MCV, mean cell corpuscular volume; MCHC, mean corpuscular hemoglobin concentration.

Additionally, at E11.5, embryo cell membranes and the cytoplasms of hepatocytes and hemocytes were fragmented (Fig. 3C).

Therefore, we evaluated the high-density materials in the mitochondria of hemocytes at E10.5 of *Abcb10*$^{-/-}$ embryos by use of analytical electron microscopy. Iron peaks were detected in high-density deposits in the mitochondria of hemocytes in an *Abcb10*$^{-/-}$ embryo but not in the mitochondria of hemocytes in an *Abcb10*$^{+/+}$ embryo (Fig. 3E).

Iron accumulation was expected to induce reactive oxygen species (ROS) production, which can be highly toxic (19, 20). We next evaluated whether iron accumulation affected protein oxidation with ROS in *Abcb10*$^{-/-}$ embryos by detecting oxidized proteins. Figure 3F shows that the oxidation level of proteins in the mitochondrial and supernatant fractions from *Abcb10*$^{-/-}$ embryos was higher than that in *Abcb10*$^{+/+}$ embryos. Collectively, these data suggest that *Abcb10* deletion induces heme biosynthesis deficiency and iron accumulation in the mitochondria of hemocytes, causing severe damage and cell death to hemocytes.

Postnatal ablation of *Abcb10* results in impaired erythroid cell maturation. To examine the physiological functions of *Abcb10*, we generated an interferon-inducible Cre transgene (Mx-Cre) to excise the floxed-*Abcb10* allele from adult mice (*Abcb10*$^{F/-}$; *Mx1-Cre*). After inducing Mx-Cre with pI-pC, an interferon inducer in hematopoietic stem cells, approximately 40% of floxed-*Abcb10* alleles in *Abcb10*$^{F/-}$; *Mx1-Cre* mouse BMCs had been converted into the deleted allele (date not shown).

Since *Abcb10*$^{-/-}$ mice show hematopoiesis failure and impairment of heme biosynthesis, we performed peripheral blood counts and estimated hemoglobin and heme concentrations in *Abcb10*$^{F/-}$; *Mx1-Cre* mice and controls (Fig. 4). Strikingly, *Abcb10*$^{F/-}$; *Mx1-Cre* mice developed anemia, as exhibited by a decrease in red blood cell (RBC) number and hemoglobin, whereas white blood cell (WBC) number and platelet count were comparable. Further, *Abcb10*$^{F/-}$; *Mx1-Cre* mice showed a marked increase in the number of reticulo-

cytes compared to the level for controls. According to the low mean corpuscular volume (MCV) and mean corpuscular hemoglobin concentration (MCHC), the anemia was classified into microcytic type and hypochromic type, which is primarily caused by impaired hemoglobin synthesis. Additionally, heme was reduced in *Abcb10*$^{F/-}$; *Mx1-Cre* mice compared with the level for controls in peripheral blood (Fig. 5A). These findings are consistent with impaired heme biosynthesis in *Abcb10*$^{F/-}$; *Mx1-Cre* mice.

Abcb10 is indispensable to heme biosynthesis. Figure 5B shows electron micrographs of controls and *Abcb10*$^{F/-}$; *Mx1-Cre* mouse BM cells. *Abcb10*$^{F/-}$; *Mx1-Cre* mitochondria showed prominent contours of the membranes and appeared to be swollen. Most mitochondria in control reticulocytes appeared to degenerate as they matured into definitive erythrocytes. The magnified *Abcb10*$^{F/-}$; *Mx1-Cre* panel shows the highly dense deposit localized in the mitochondria. Additionally, diffuse deposition was observed in the matrix (Fig. 5B, arrowheads). No comparable electron densities were observed in controls (note the presence of intracellular organelles). An appearance in electron micrographs similar to that of *Abcb10*$^{-/-}$ mice and analytical electron microscopy data for *Abcb10*$^{-/-}$ mice suggested that these deposits were the result of iron accumulation.

To examine the impaired step of heme biosynthesis, we evaluated the concentration of the heme precursor PPIX and observed that PPIX concentrations in *Abcb10*$^{F/-}$; *Mx1-Cre* mice were more than 50 times higher than those in the control mice (Fig. 5C). Thus, PPIX accumulation in *Abcb10*$^{F/-}$; *Mx1-Cre* mice suggests that iron utilization was defective. Collectively, these data suggest that *Abcb10* plays an essential role in incorporating iron into PPIX during heme biosynthesis.

DISCUSSION

Abcb10$^{-/-}$ mice were embryonic lethal between E10.5 and E11.5. These embryos appeared to be paler in the absence of erythropoi-
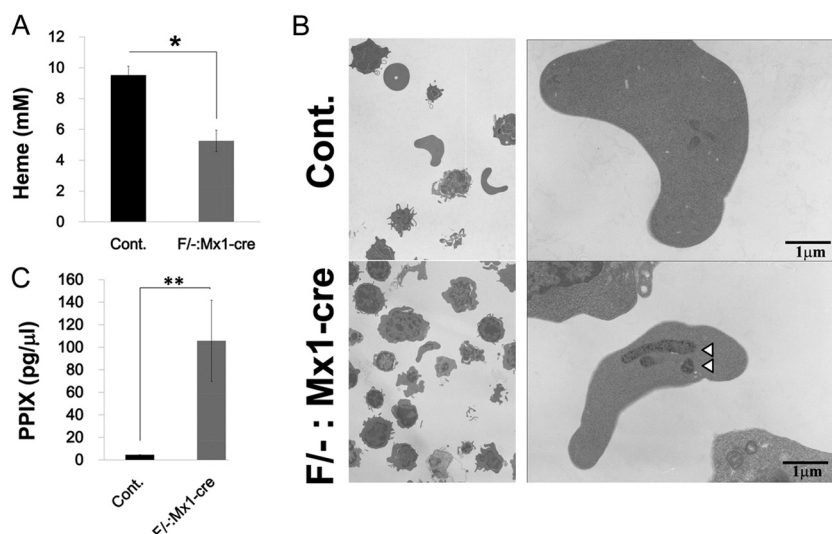
FIG 5 Deletion of *Abcb10* in hematopoietic cells leads to heme biosynthesis deficiency. (A and C) Determination heme and PPIX concentrations in peripheral blood from control ($n = 3$) and *Abcb10*^F/−^; *Mx1-Cre* ($n = 9$) mice. Results are shown as means ± SDs (error bars). (B) Electron micrographs of bone marrow cells in control and *Abcb10*^F/−^; *Mx1-Cre* mice. Arrowheads show strong electron-dense deposits in the matrix of mitochondria of *Abcb10*^F/−^; *Mx1-Cre* cells.

esis than in its presence. These phenomena are consistent with the phenotype of erythrocyte deficiency, similar to what has been observed for *Gata1* KO mice (21, 22). The concentration of oxidized protein in *Abcb10*^−/−^ mice was much higher than that in normal mice. These results suggest that *Abcb10* deficiency induces production of ROS and damage to proteins. *Abcb10*^F/−^; *Mx1-Cre* mice suffered from severe anemia with accumulation of PPIX and iron in erythroid cells. The numbers of WBCs and platelets are comparable to those in normal controls, suggesting that *Abcb10* deficiency did not affect hematopoietic cells other than erythroid cells. These findings are consistent with the function of ABCB10 as a scaffold protein of FECH and the SLC25A37 complex on the mitochondrial inner membrane (9). Although the level of Fech protein in mitochondria in the *Abcb10*^−/−^ mice was comparable to that in the wild-type mice, heme biosynthesis stopped, and its precursor iron and PPIX were accumulated. These data suggest that Abcb10 might also be involved in the protein stability of Slc25a37; furthermore, Abcb10 might function not only as a scaffold protein but also as a part of heme biosynthesis machinery with Fech and Slc25a37.

Although *Abcb10*^+/−^ mice showed an increased susceptibility to oxidative stress caused by ischemia/reperfusion, we did not observe clear morphological or hematological changes between *Abcb10*^+/−^ and *Abcb10*^+/+^ mice (13). Upon a sudden increase in ROS production, *Abcb10*^+/−^ mice are thought to have an insufficient capacity to adapt to this rapid metabolic change. It remains unclear whether *Abcb10*^+/−^ mice are unable to produce heme proteins such as catalase and dismutase, which protect tissues from oxidative stress, or whether *Abcb10* plays other roles in reducing ROS production in mitochondria. Further studies are needed to clarify these points.

Two major congenital diseases related to heme biosynthesis are protoporphyria and sideroblastic anemia (SA). Protoporphyria is a disorder caused by protoporphyrin accumulation due to partial deficiency of metabolic enzymes in the heme biosynthesis pathway. EPP is a major type of protoporphyria caused by low enzyme activity of FECH with genetic abnormality. Two mouse models,

consisting of heterozygotes of mice with *Fech* exon 10 deleted and homozygous *Fech*^m1pas^ mice containing the point mutation M98K in the *Fech* protein, have been reported. The protoporphyria-like phenotypes of these mice are consistent with low Fech enzyme activity (23–25). In contrast, *ALAS2* is known to be a major causative gene of XLSA. Heterozygous *Alas2* KO mice show a normal phenotype, while *Alas2* homozygous KO mice and X-linked pseudohemizygous *Alas2*^−/y^ mice show embryonic lethality; ring sideroblasts were not observed in mouse embryos (26). A transgenic mouse whose *Alas2* activity was partially rescued in an *Alas2*-null background was reported to be a model of human XLSA (27). Since both of these diseases are rare, it is more difficult to establish effective treatments for them than for common diseases. Therefore, animal models are very useful for treatment evaluation. It has been reported that 43% of human congenital SA cases are caused by unidentified genes or mutations (28).

We found that *Abcb10* is essential for heme biosynthesis and that *Abcb10*^−/−^ mice have pathological conditions, including iron accumulation in the mitochondria and PPIX accumulation, similar to those of SA and EPP. These findings indicate that mutations in *Abcb10* may modify these hematopoietic diseases since the *Abcb10* homozygous deletion showed wide effects on function in the heme biosynthesis cascade and erythroblast differentiation. However, there have been no reports showing abnormalities in *ABCB10* in human SA and EPP (28, 29). This discrepancy between our finding and the results of human genetic analysis can be explained by the complex combination of genetic abnormalities and/or the difficulty of genetic and epidemiologic analysis of SA because of its rarity and the variety of symptoms and severities caused by the disease (30, 31). Crossbreeding of *Abcb10* heterozygous deletion mice with KO mice carrying other heme synthesis-related genes may provide important clues regarding the genetic background of heme synthesis abnormalities.

ACKNOWLEDGMENTS

REFERENCES

1. **Hamza I.** 2006. Intracellular trafficking of porphyrins. ACS Chem. Biol. **1**:627–629. http://dx.doi.org/10.1021/cb600442b.

2. **Cotter PD, Rucknagel DL, Bishop DF.** 1994. X-linked sideroblastic anemia: identification of the mutation in the erythroid-specific delta-aminolevulinate synthase gene (ALAS2) in the original family described by Cooley. Blood **84**:3915–3924.

3. **Yamamoto M, Nakajima O.** 2000. Animal models for X-linked sideroblastic anemia. Int. J. Hematol. **72**:157–164.

4. **Cox TM.** 1997. Erythropoietic protoporphyria. J. Inherit Metab. Dis. **20**:258–269. http://dx.doi.org/10.1023/A:1005317124985.

5. **Chen W, Paradkar PN, Li L, Pierce EL, Langer NB, Takahashi-Makise N, Hyde BB, Shirihai OS, Ward DM, Kaplan J, Paw BH.** 2009. Abcb10 physically interacts with mitoferrin-1 (Slc25a37) to enhance its stability and function in the erythroid mitochondria. Proc. Natl. Acad. Sci. U. S. A. **106**:16263–16268. http://dx.doi.org/10.1073/pnas.0904519106.

6. **Sassa S, Kappas A.** 2000. Molecular aspects of the inherited porphyrias. J. Intern. Med. **247**:169–178. http://dx.doi.org/10.1046/j.1365-2796.2000.00618.x.

7. **Shaw GC, Cope JJ, Li L, Corson K, Hersey C, Ackermann GE, Gwynn B, Lambert AJ, Wingert RA, Traver D, Trede NS, Barut BA, Zhou Y, Minet E, Donovan A, Brownlie A, Balzan R, Weiss MJ, Peters LL, Kaplan J, Zon LI, Paw BH.** 2006. Mitoferrin is essential for erythroid iron assimilation. Nature **440**:96–100. http://dx.doi.org/10.1038/nature04512.

8. **Troadec MB, Warner D, Wallace J, Thomas K, Spangrude GJ, Phillips J, Khalimonchuk O, Paw BH, Ward DM, Kaplan J.** 2011. Targeted deletion of the mouse Mitoferrin1 gene: from anemia to protoporphyria. Blood **117**:5494–5502. http://dx.doi.org/10.1182/blood-2010-11-319483.

9. **Chen W, Dailey HA, Paw BH.** 2010. Ferrochelatase forms an oligomeric complex with mitoferrin-1 and Abcb10 for erythroid heme biosynthesis. Blood **116**:628–630. http://dx.doi.org/10.1182/blood-2009-12-259614.

10. **Shirihai OS, Gregory T, Yu C, Orkin SH, Weiss MJ.** 2000. ABC-me: a novel mitochondrial transporter induced by GATA-1 during erythroid differentiation. EMBO J. **19**:2492–2502. http://dx.doi.org/10.1093/emboj/19.11.2492.

11. **Graf SA, Haigh SE, Corson ED, Shirihai OS.** 2004. Targeting, import, and dimerization of a mammalian mitochondrial ATP binding cassette (ABC) transporter, ABCB10 (ABC-me). J. Biol. Chem. **279**:42954–42963. http://dx.doi.org/10.1074/jbc.M405040200.

12. **Tang L, Bergevoet SM, Bakker-Verweij G, Harteveld CL, Giordano PC, Nijtmans L, de Witte T, Jansen JH, Raymakers RA, van der Reijden BA.** 2011. Human mitochondrial ATP-binding cassette transporter ABCB10 is required for efficient red blood cell development. Br. J. Haematol. **157**:151–154. http://dx.doi.org/10.1111/j.1365-2141.2011.08936.x.

13. **Liesa M, Luptak I, Qin F, Hyde BB, Sahin E, Siwik DA, Zhu Z, Pimentel DR, Xu XJ, Ruderman NB, Huffman KD, Doctrow SR, Richey L, Colucci WS, Shirihai OS.** 2011. Mitochondrial transporter ATP binding cassette mitochondrial erythroid is a novel gene required for cardiac recovery after ischemia/reperfusion. Circulation **124**:806–813. http://dx.doi.org/10.1161/CIRCULATIONAHA.110.003418.

14. **Hyde BB, Liesa M, Elorza AA, Qiu W, Haigh SE, Richey L, Mikkola HK, Schlaeger TM, Shirihai OS.** 2012. The mitochondrial transporter ABC-me (ABCB10), a downstream target of GATA-1, is essential for erythropoiesis in vivo. Cell Death Differ. **19**:1117–1126. http://dx.doi.org/10.1038/cdd.2011.195.

15. **Yamamoto M, Yaginuma K, Tsutsui H, Sagara J, Guan X, Seki E, Yasuda K, Yamamoto M, Akira S, Nakanishi K, Noda T, Taniguchi S.** 2004. ASC is essential for LPS-induced activation of procaspase-1 independently of TLR-associated signal adaptor molecules. Genes Cells **9**:1055–1067. http://dx.doi.org/10.1111/j.1365-2443.2004.00789.x.

16. **MacDonald MJ.** 1995. Feasibility of a mitochondrial pyruvate malate shuttle in pancreatic islets. Further implication of cytosolic NADPH in insulin secretion. J. Biol. Chem. **270**:20051–20058.

17. **Lim CK.** 2002. Analysis of biosynthetic intermediates, 5-aminolevulinic acid to heme, p 95–109. *In* Smith AG, Witty M (ed), Heme, chlorophyll, and billins. Humana Press, Totowa, NJ.

18. **Samokhvalov IM, Samokhvalova NI, Nishikawa S.** 2007. Cell tracing shows the contribution of the yolk sac to adult haematopoiesis. Nature **446**:1056–1061. http://dx.doi.org/10.1038/nature05725.

19. **Eaton JW, Qian M.** 2002. Molecular bases of cellular iron toxicity. Free Radic. Biol. Med. **32**:833–840. http://dx.doi.org/10.1016/S0891-5849(02)00772-4.

20. **Harigae H, Nakajima O, Suwabe N, Yokoyama H, Furuyama K, Sasaki T, Kaku M, Yamamoto M, Sassa S.** 2003. Aberrant iron accumulation and oxidized status of erythroid-specific delta-aminolevulinate synthase (ALAS2)-deficient definitive erythroblasts. Blood **101**:1188–1193. http://dx.doi.org/10.1182/blood-2002-01-0309.

21. **Fujiwara Y, Browne CP, Cunniff K, Goff SC, Orkin SH.** 1996. Arrested development of embryonic red cell precursors in mouse embryos lacking transcription factor GATA-1. Proc. Natl. Acad. Sci. U. S. A. **93**:12355–12358. http://dx.doi.org/10.1073/pnas.93.22.12355.

22. **Shivdasani RA, Fujiwara Y, McDevitt MA, Orkin SH.** 1997. A lineage-selective knockout establishes the critical role of transcription factor GATA-1 in megakaryocyte growth and platelet development. EMBO J. **16**:3965–3973. http://dx.doi.org/10.1093/emboj/16.13.3965.

23. **Magness ST, Maeda N, Brenner DA.** 2002. An exon 10 deletion in the mouse ferrochelatase gene has a dominant-negative effect and causes mild protoporphyria. Blood **100**:1470–1477. http://dx.doi.org/10.1182/blood-2001-12-0283.

24. **Tutois S, Montagutelli X, Da Silva V, Jouault H, Rouyer-Fessard P, Leroy-Viard K, Guénet JL, Nordmann Y, Beuzard Y, Deybach JC.** 1991. A recessive inherited ferrochelatase deficiency with anemia, photosensitivity, and liver disease. J. Clin. Invest. **88**:1730–1736. http://dx.doi.org/10.1172/JCI115491.

25. **Boulechfar S, Lamoril J, Montagutelli X, Guenet JL, Deybach JC, Nordmann Y, Dailey H, Grandchamp B, de Verneuil H.** 1993. Ferrochelatase structural mutant (Fechm1Pas) in the house mouse. Genomics **16**:645–648. http://dx.doi.org/10.1006/geno.1993.1242.

26. **Nakajima O, Takahashi S, Harigae H, Furuyama K, Hayashi N, Sassa S, Yamamoto M.** 1999. Heme deficiency in erythroid lineage causes differentiation arrest and cytoplasmic iron overload. EMBO J. **18**:6282–6289. http://dx.doi.org/10.1093/emboj/18.22.6282.

27. **Nakajima O, Okano S, Harada H, Kusaka T, Gao X, Hosoya T, Suzuki N, Takahashi S, Yamamoto M.** 2006. Transgenic rescue of erythroid 5-aminolevulinate synthase-deficient mice results in the formation of ring sideroblasts and siderocytes. Genes Cells **11**:685–700. http://dx.doi.org/10.1111/j.1365-2443.2006.00973.x.

28. **Bergmann AK, Campagna DR, McLoughlin EM, Agarwal S, Fleming MD, Bottomley SS, Neufeld EJ.** 2010. Systematic molecular genetic analysis of congenital sideroblastic anemia: evidence for genetic heterogeneity and identification of novel mutations. Pediatr. Blood Cancer **54**:273–278. http://dx.doi.org/10.1002/pbc.22244.

29. **Saito S, Iida A, Sekine A, Miura Y, Ogawa C, Kawauchi S, Higuchi S, Nakamura Y.** 2002. Three hundred twenty-six genetic variations in genes encoding nine members of ATP-binding cassette, subfamily B (ABCB/MDR/TAP), in the Japanese population. J. Hum. Genet. **47**:38–50. http://dx.doi.org/10.1007/s10038-002-8653-6.

30. **Furuyama K, Harigae H, Kinoshita C, Shimada T, Miyaoka K, Kanda C, Maruyama Y, Shibahara S, Sassa S.** 2003. Late-onset X-linked sideroblastic anemia following hemodialysis. Blood **101**:4623–4624. http://dx.doi.org/10.1182/blood-2002-09-2804.

31. **Harigae H, Furuyama K.** 2010. Hereditary sideroblastic anemia: pathophysiology and gene mutations. Int. J. Hematol. **92**:425–431. http://dx.doi.org/10.1007/s12185-010-0688-4.